Advanced Functional Materials

ADVANCED FUNCTIONAL MATERIALS
www.afm-journal.de

RESEARCH ARTICLE OPEN ACCESS

Sensitized Triplet Exciton Generation in Nanostructured Polymer Scintillators: Toward Improved γ/Neutron Discrimination

Luca Pollice[1] | Xueqian Hu[2] | Letizia G. Tedoldi[3] | Andrea Erroi[1] | Davide Rigamonti[4] | Marco Tardocchi[4] | Davide Bortot[5] | Andrea Pola[5] | Christoph Weder[2] | Angelo Monguzzi[1]

[1]Department of Materials Science, University of Milano-Bicocca, Milano, Italy | [2]Adolphe Merkle Institute, University of Fribourg, Fribourg, Switzerland | [3]Department of Physics, University of Milano-Bicocca, Milano, Italy | [4]Institute for Plasma Science and Technology, National Research Council of Italy, Milano, Italy | [5]Department of Energy- Nuclear Engineering Division, Polytechnic of Milan, Milano, Italy

Correspondence: Angelo Monguzzi (angelo.monguzzi@unimib.it)

Received: 11 February 2026 | **Revised:** 3 March 2026 | **Accepted:** 5 March 2026

ABSTRACT

Scintillating materials emit light when exposed to ionizing radiation and are particularly useful for the detection of nuclear threats, medical imaging, and high-energy physics. A subset of these materials enables the discrimination of neutrons and charged particles from γ-rays through pulse shape discrimination (PSD). This time-gated technique exploits that in these materials, the scintillation pulse shape depends on the nature of the incident radiation. The most used PSD materials are polymeric scintillators featuring triplet–triplet annihilation (TTA) based delayed fluorescence as the radiation fingerprint. We report here that sensitive and rapid PSD is achieved in nanostructured polymeric scintillators consisting in a solid polymer matrix and liquid nanodomains in which the TTA-active dye 9,10 diphenyl anthracene is dissolved. The liquid nature of the nanodomains renders TTA highly efficient, allowing delayed fluorescence to occur at low energy densities. We demonstrate that TTA is further enhanced by the inclusion of properly selected and dosed metalated porphyrin. The latter act as γ/neutron discrimination sensitizers, doubling the density of annihilating triplets and increasing the time discrimination capability by 30% at event rates up to 1 MHz. Interestingly, these improvements are related to a sensitization effect that does not involve triplet-triplet energy transfer from metalated porphyrins.

1 | Introduction

Conjugated molecules capable of triplet-triplet annihilation (TTA) are ideal candidates to be used as scintillators for the detection and discrimination of high-energy neutrons in the presence of a strong γ-ray background. This capability is crucial for non-proliferation and detection of nuclear threats [1, 2] as well as in high-energy physics experiments [3, 4]. Owing to their high hydrogen content, conjugated materials exhibit a large interaction cross-section with fast neutrons, resulting in an efficient stopping power [5]. In these materials, γ/neutron discrimination is achieved through scintillation pulse shape discrimination (PSD), which exploits differences in the intensity decay time of the light pulses generated by the simultaneous interaction of the scintillator with neutrons and γ-rays (Figure 1a). The luminescence signal consists of a prompt emission due to radiative recombination of singlet excited states S_1^* and in a delayed emission, which arises from the population of S_1^* states via TTA between triplet excitons T_1^* (Figure 1b) [6, 7]. The relative intensity and decay kinetics of the two components reflect the TTA rate and yield [8–11]. γ-Rays in conjugated materials deposit energy through Compton scattering over extended regions, which

Luca Pollice and Xueqian Hu contributed equally to this work.

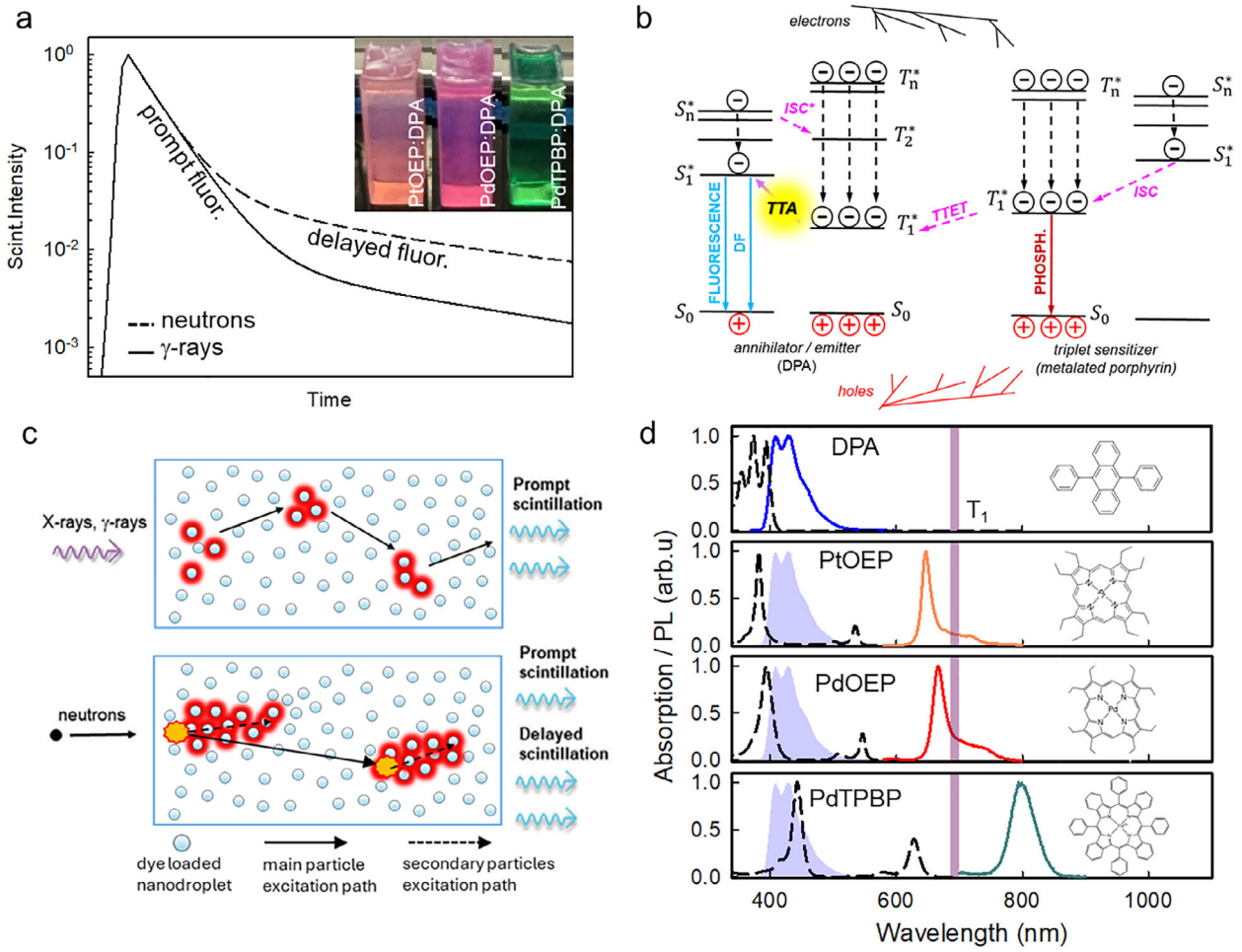

FIGURE 1 | a) Concept of the pulse shape discrimination technique (PSD) used to distinguish high-energy photons (X-rays, γ-rays), which cause prompt emission, from neutrons, which promote TTA-based, delayed emission. The time-gated analysis of scintillation pulses allows discriminating the type of incident radiation. The inset is a digital picture of representative samples of nanostructured scintillators loaded with *porphyrin*:DPA. b) Schematic of energetic pathways involved in the (sensitized) TTA mechanism. The delayed fluorescence (DF) produced by TTA of two annihilator/emitter dyes can be sensitized by a triplet sensitizer moiety, usually a metalated porphyrin. The energy stored in the metalated porphyrin triplet state formed upon charge recombination or by intersystem crossing (ISC) from the singlet state is transferred to the annihilator triplets through non-radiative energy transfer (TTET), thus enhancing the production of delayed emission. ISC* marks the ISC induced on the excited DPA dyes by the metalated porphyrins due to an intermolecular heavy metal effect, which also enhances the formation of DPA triplets. Solid lines represent radiative, dashed lines non-radiative transitions. c) Sketch of the different interaction mechanisms of the nanostructured polymer scintillators with high-energy photons (X-rays, γ-rays) or fast neutrons. d) Molecular structures, normalized optical absorption (black dashed lines), and photoluminescence spectra of the investigated metalated porphyrins PtOEP (orange), PdOEP (red), and PdTPBP (blue) in butyl benzoate (BuBz) solution (10^{-4} M) and the annihilator/emitter DPA (10^{-4} M in BuBz). The shaded purple region represents the energy of the DPA's dark triplet state T_1.

favors the formation of S_1^* states, mainly causing prompt emission (Figure 1c, top) [12]. Fast neutrons, conversely, undergo inelastic scattering with hydrogen atoms, producing energetic protons that lose their energy in a very localised volume, mainly leading to the formation of T_1^* states (Figure 1c, bottom). Thus, the neutron-induced scintillation shows an evident delayed component, which allows for PSD with respect to the γ-rays scintillation events [13–15].

Organic crystals or liquid solutions of fluorescent molecules in organic solvents can be used as γ/neutron discriminators [14, 16, 17]. Both systems exhibit high triplets diffusivity (up to 10^{-5} cm^2 s^{-1} in liquids and up to 10^{-3} cm^2 s^{-1} in crystals) [18] which enhances the TTA yield, resulting in a good PSD performance. However, organic crystals are expensive and fragile, while liquid scintillators are not easy to handle, often posing dangers due to flammability and toxicity, and the disposal of radioactive liquids is somewhat cumbersome [13]. An inexpensive solution that affords mechanically robust materials is the use of conjugated dye-loaded scintillating polymers. Zaitseva et al. demonstrated in 2012 the ability of these systems as γ/neutron discriminators [19]. By heavily loading a polymeric host with TTA-active fluorescent dyes, their intermolecular distance can be reduced down to ~10 Å [20]. This partially overcomes the limited molecular diffusivity in rigid amorphous polymers (~10^{-14} cm^2 s^{-1}) [21], by allowing a slow triplet hopping process in which their diffusion is driven by intermolecular Dexter energy transfer. However, the resulting TTA process is slow and poorly efficient. This is a crucial drawback of polymeric PSD scintillators, which have limited sensitivity and struggle with high counting rates due to pile-up

[22]. Thus, their application is restricted, especially with respect to the discrimination of high-rate events (>>100 kHz).

We recently demonstrated that fast delayed emission and γ/neutron PSD can be achieved in nanostructured multiphase polymer scintillator materials [23]. As shown in Figure 1c, these transparent materials are composed of a glassy polymeric matrix containing homogenously dispersed liquid nanodomains (i.e. nanodroplets) in which a TTA active dye is dissolved [24, 25]. This architecture offers several advantages. First, the TTA-active molecules diffuse quickly within the nanodroplets, enabling fast TTA. Second, since the molecules are confined within a volume much smaller than their triplet diffusion length, the diffusivity limit condition is fulfilled. Thus, this confined-TTA regime ensures a 100% probability of TTA, provided that two triplets are excited within the same droplet [25, 26]. Intriguingly, we observed that the incorporation of a metalated phosphorescent porphyrin in the droplets, originally thought to act only as a triplet sensitizer (Figure 1b), positively affects the PSD properties of the material [23, 27, 28].

Originally with the goals of demonstrating the versatility of the design approach, including the possibility of simultaneously incorporating different sensitizer-emitter pairs and exploiting the energy nanoconfinement to further enhance the system performance, we embarked on a systematic investigation of this sensitized scintillation PSD mechanism in nanostructured polymers. We combined the TTA-active dye 9,10 diphenyl anthracene (DPA, Figure 1d) [29] with three phosphorescent metalated porphyrins. Two of these porphyrins are capable of efficient triplet-triplet energy transfer (TTET) to DPA, but they contain metal ions with different atomic numbers, i.e., platinum (Pt) and palladium (Pd), respectively. The third porphyrin contains Pd, but its triplet state energies are off resonance with respect to the DPA, so that TTET is not permitted. This allowed us to isolate the effect of the heavy metal ion in the nanoscale energy reservoirs and to assess the importance of the sensitizer-to-annihilator energy transfer contribution. We found that the addition of a metalated porphyrin into the nanodroplets, which has a diameter of 40 nm, [23] effectively improves the γ/neutron discrimination, surprisingly, regardless of its ability for TTET to DPA, provided that it is added at a concentration not exceeding ca. 10^{-6} M. At higher concentrations, parasitic processes such as reabsorption and singlet or triplet back energy transfers (BET) from the emitters/annihilators to the sensitizers become significant, leading to a reduction in the overall emission intensity [30]. These findings highlight the beneficial role of heavy metal atoms in improving γ/neutron PSD, while also underscoring the importance of concentration-dependent mechanisms, particularly effective in systems where molecular species are confined within nanoscopic domains.

2 | Results and Discussion

2.1 | Absorption, Luminescence and Scintillation Properties of the Nanostructured Polymers

Figure 1d shows the UV–vis absorption and emission spectra of the compounds involved in the study, measured in diluted butyl benzoate solutions. The DPA dye is a blue-emitting fluorophore with a photoluminescence quantum yield (PLQY) of 0.96 [29]. Its $S_0 - T_1$ energy gap is 1.77 eV, which corresponds to a wavelength of ~700 nm. The porphyrins evaluated as triplet sensitizers are palladium octaethylporphyrin (PdOEP), platinum octaethylporphyrin (PtOEP), and meso-tetraphenyl tetrabenzoporphine palladium (PdTPBP). Under UV or visible excitation, PtOEP and PdOEP are phosphorescent, emitting photons in the red-NIR part of the electromagnetic spectrum at 645 and 665 nm, respectively. They both exhibit efficient TTET toward the DPA triplets T_1, and can thus increase the number of annihilating T_1^* states in each nanodroplet through an energy transfer pathway [31]. PtOEP contains a platinum atom (atomic number Z = 76), which is much heavier than the palladium (Z = 46) present in the other two porphyrins. We therefore expected a different interaction with the ionizing radiation and particles depending on the Z value [5, 32, 33]. The emission of PdTPBP is red-shifted relative to the other two porphyrins, with a phosphorescence maximum in the NIR at 800 nm. This value is significantly lower than the DPA triplet energy, preventing TTET. As such, any effect imparted on the scintillation is purely due to the presence of the heavy element, and not due to an increase in triplet density via the sensitization mechanism possible in the other systems. The nanostructured plastic scintillators were prepared according to previously reported procedures [23, 25]. They consist of a matrix polymer formed by radical copolymerization of the polar monomers methacrylic acid, 2-hydroxyethyl methacrylate, and triethylene glycol dimethacrylate, and contain 10 wt.% of liquid butyl benzoate in the form of nanodroplets. The structure formation is facilitated by the use of a plasticizer and a surfactant (Experimental Section). Three different series of scintillating materials, based on the three metal porphyrins, were investigated. Each metal complex was used in three different concentrations (2×10^{-5} M, 2×10^{-6} M, and 2×10^{-7} M) and paired with DPA, whose concentration was fixed at 1.5×10^{-2} M. These concentrations are quoted with respect to the overall volume of the reaction mixture, and their concentration in the nanodroplets is roughly an order of magnitude higher, assuming that the dyes exclusively reside in the nonpolar solvent [24, 26]. Reference samples containing only DPA ($c = 1.5 \times 10^{-2}$ M) or only the metal complexes ($c = 2 \times 10^{-5}$ M) were made in the same way. We selected $c = 2 \times 10^{-5}$ M as the starting concentration, which is the maximum at which scintillation with an adequate intensity is observed. The emission intensity is reduced at higher metal complex concentrations, rendering a comparative analysis difficult (Figure S1).

Prior to any scintillation experiments, the photophysical properties of the nanostructured scintillators were investigated using UV–vis absorption, steady-state, and time-resolved photoluminescence spectroscopy. All scintillators exhibit absorption spectra that match those of DPA and the porphyrins in solution, and the shapes of the respective photoluminescence spectra are identical (Figures S2 and S3), indicating that the incorporation of the dyes does not lead to the formation of aggregates or excimers. Upon excitation at the lowest energy absorption band of the respective porphyrin, the polymers containing both DPA and sensitizers show weak emission with maxima at 645, 665, and 800 nm for PtOEP:DPA, PdOEP:DPA, and PdTPBP:DPA, respectively. By comparing the phosphorescence intensity of materials with (I_{Ph}) and without (I_{Ph}^0) DPA (Figure S4), it is possible to estimate the TTET efficiency as $\phi_{ET} = 1 - (I_{Ph}/I_{Ph}^0)$ [35]. PtOEP and PdOEP efficiently transfer their energy to the DPA with an efficiency

~0.90 (measured at a porphyrin concentration of 2×10^{-5} M), demonstrating that the majority of the dyes is located within the droplets and in close enough proximity for an efficient TTET [25]. In the case of PdTPBP, the phosphorescence intensity does not change in the presence of DPA, indicating a $\phi_{ET} = 0$. The analysis of the DPA fluorescence intensity decay at 430 nm under pulsed UV excitation (Figure S5) shows that the addition of porphyrins causes a decrease in the intrinsic DPA fluorescence decay time of 9 ns, which becomes more pronounced as the concentration of the porphyrin increases [29]. This is due to the partial resonance between the DPA emission and the absorption of the porphyrins in the blue spectral region, which causes a singlet-singlet BET. The BET efficiency is calculated as $\phi_{BET} = 1 - (\tau/\tau_0)$ [36], where τ and τ_0 are the DPA lifetimes in the presence and absence of the porphyrins, respectively [8]. At the highest porphyrin concentration employed (2×10^{-5} M), ϕ_{BET} increases up to 25%, regardless of the type of sensitizer (Table S1). This suggests that the effective resonance between the energy acceptor absorption and the energy donor emission does not affect the BET yield, which, as expected, is determined by the confinement of the dyes in the liquid nanodomains.

The scintillation properties of nanostructured polymers were first probed by radioluminescence (RL) emission spectroscopy under continuous irradiation with soft X-rays (Experimental Section). Figure 2a shows the samples' RL spectra, acquired in reflection mode. At the highest porphyrin concentration of 2×10^{-5} M, a reduction of the DPA blue emission intensity is observed in all samples, due to partial reabsorption or BET processes (insets of Figure 2a). This detrimental effect is most pronounced in samples containing PdTPBP, where reabsorption of DPA fluorescence is critical, leading to a 50% reduction in the emission intensity. No significant effects are observed at lower porphyrin concentrations (2×10^{-6} M and 2×10^{-7} M), in agreement with the limited re-absorption and BET effects. The scintillation of these samples was then tested under exposure to γ-ray emitted from a ^{60}Co source (Experimental Section). Figure 2b shows the recorded energy spectra. On the *x*-axis, the number of channels activated by the scintillation light is proportional to the emission intensity of the material and its light yield (LY), i.e. the number of photons emitted per unit of energy deposited by the ionizing radiation. Since no photoelectric peak can be observed due to the low density of the material [5], the scintillator relative yield can be evaluated by comparing the values of the Compton edge position (Experimental Section, Table S2) [37]. The values obtained are consistent with the behavior of the relative RL intensities reported in the insets of Figure 2a, confirming the detrimental effects of reabsorption and BET, which limit scintillation light output at concentrations above 10^{-6} M, especially for materials containing PdTPBP.

2.2 | γ/Neutron PSD of the Nanostructured Polymer Scintillators

The PSD capability of the nanostructured polymers was tested by exposing the samples to an americium-beryllium (AmBe) source, which emits both γ-rays and fast neutrons with energies between 1 and 8 MeV [38]. Figure 3 shows the PSD plots obtained by applying the charge integration method on the recorded scintillation pulses (Experimental Section). For every sample, two peaks can be identified. The first one, located at PSD values around 0.1, is associated with γ-rays. The second, at higher PSD values around 0.3, is associated with fast neutrons. As shown in Figure 4, the projections of the PSD plots on the *y*-axis can be fitted with a double Gaussian peak function, yielding the exact PSD values for γ-rays and neutrons. All PSD projection plots are directly comparable, as detailed in the Experimental Section. The difference in the mean values of the two Gaussians (Δ_{PSD}) together with the full width at the half maximum (FWHM) of the peaks are the two key parameters to evaluate the γ/neutron discrimination capability, by calculating the discrimination figure of merit FOM $= \frac{\Delta_{PSD}}{FWHM_\gamma + FWHM_n}$ [13]. The FOM values of each scintillator are reported in Tables S3–S5. The data show that while a slight improvement in the FOM is observed for some compositions, the effect is not significant, as the LY of the scintillators is far from optimized, which limits the effective light output. As a consequence, the data shown in Figure 3 exhibits a low signal-to-noise ratio, which in turn significantly affects the FWHM of the two Gaussian peaks. Nevertheless, interesting observations can be made when considering the Δ_{PSD} values. The reference sample containing only DPA shows a Δ_{PSD} of 0.125, which is significantly larger than the 0.05 measured for the commercial reference PSD scintillator EJ-276D under the same experimental conditions (Figure S6). The addition of 2×10^{-5} M of metalated porphyrins induces a loss in the emission intensity, which is particularly deleterious in the case of PdTPBP, where it is not even possible to estimate the Δ_{PSD} due to the lack of emission (Figure S7). By contrast, a slight increase in the Δ_{PSD} of up to 0.136 is observed for PtOEP, while for the PdOEP no significant variations in efficiency are noted (Table S3). Better results are obtained by reducing the concentration of porphyrins to 2×10^{-6} M. Indeed, a general increase in light emission and discrimination efficiency is observed (Figure 4b; Table S4), due to the fact that parasitic re-absorption and BET mechanisms are reduced.

Notably, the highest Δ_{PSD} of 0.163 is achieved using the PdTPBP, a value that is more than 3 times larger than the one measured for the reference EJ-276D. By further reducing the porphyrin concentration to 2×10^{-7} M, a significant difference in Δ_{PSD} is still observed with respect to the DPA only reference sample (0.125), with Δ_{PSD} values of 0.143, 0.148, and 0.154 for PtOEP, PdOEP, and PdTPBP respectively (Table S5). Thus, no significant difference is observed between TTET-active or inactive porphyrins, suggesting that the increase in Δ_{PSD} is related to an effect of the heavy metal that does not involve TTET. These findings reveal two important facts. First, the nanostructuration of the host polymer has a significant effect on the TTA yield, resulting in a ΔPSD that is significantly better than that of a commercial solid reference material. Second, the presence of the metalated porphyrin leads to a larger production of annihilating triplets in the system, which enables an even better Δ_{PSD} discrimination with respect to the porphyrin-free system. However, this increase appears not to be due to TTET from the porphyrin triplets to the DPA [9, 10]. Because the porphyrin concentration is small, the density of the materials does not change significantly and the improved PSD behavior does not result from an increased stopping power. Moreover, the improvement is also observed for materials containing PdTPBP, which cannot transfer triplets to DPA. Therefore we

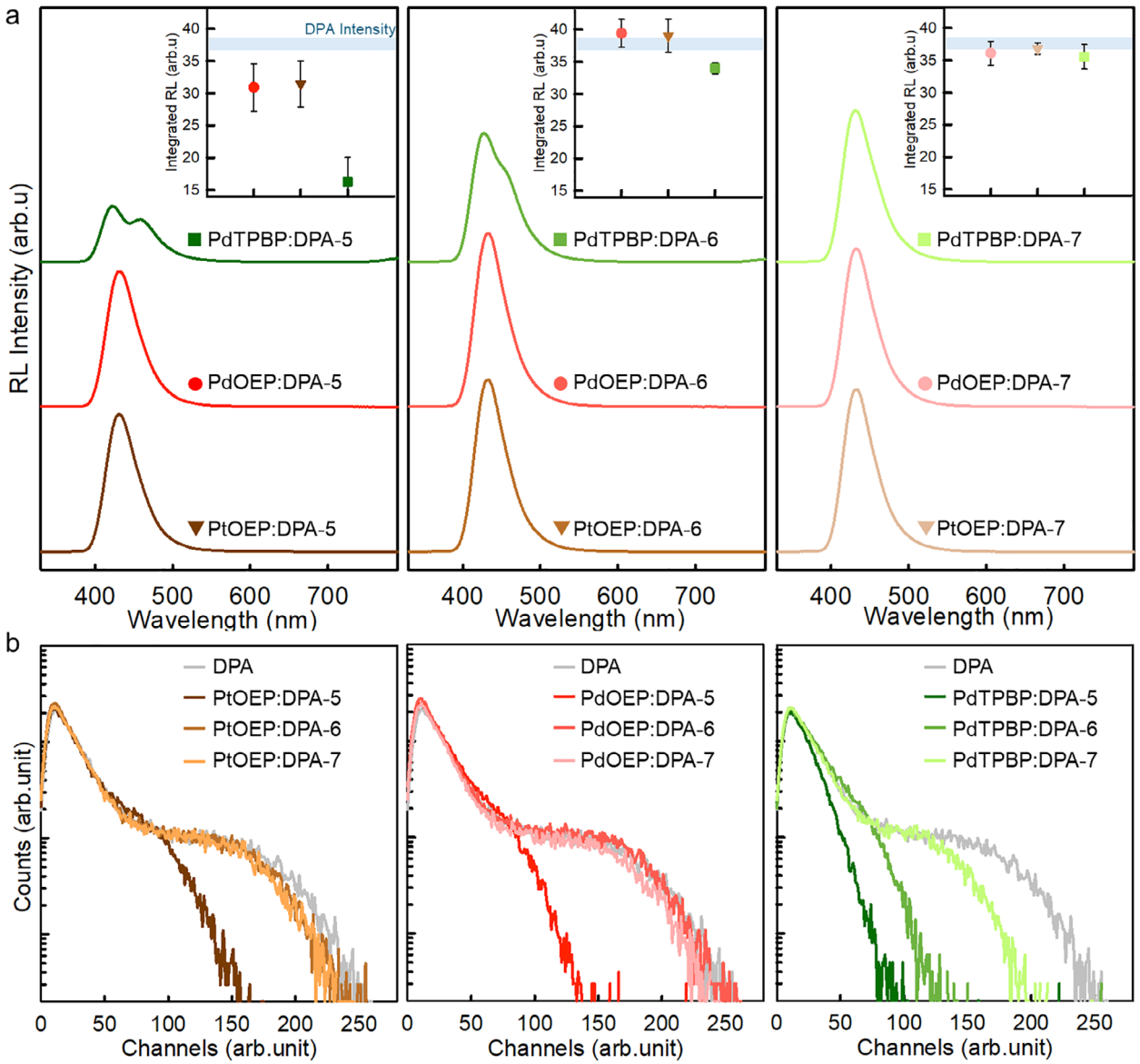

FIGURE 2 | a) Radioluminescence (RL) spectra of the nanostructured polymer scintillators investigated, recorded under exposure with soft X-rays. The concentration of DPA (1.5×10^{-2} M) was kept constant. The concentration of the porphyrins was 2×10^{-5} M, 2×10^{-6} M, or 2×10^{-7} M; samples are coded *porphyrin*:DPA-5, -6 and -7, respectively. The insets show the relative integrated RL intensities. b) Scintillation pulse height spectra under ^{60}Co radiation source of the same materials. All concentrations are quoted relative to the overall compositions.

conclude that the larger DPA triplet production is the result of an intermolecular heavy metal effect [39, 40]. Indeed, the close proximity of excited DPA molecules and the metal porphyrins affects the probability of the singlet-to-triplet generation on DPA by intersystem crossing between hot states during the scintillation process. This effect shifts the DPA population toward the triplet state and enhances the delayed fluorescence generation by TTA.

To study the effect of porphyrin addition on the scintillation kinetics and delayed emission intensity in more detail, we extracted the scintillation pulses obtained under AmBe irradiation. Scintillation pulse waveforms for each sample were obtained from the two regions of interest (ROI) in the PSD plot associated with γ-ray and neutron events, respectively (Experimental Section). First, we analyzed the waveforms of the γ-ray ROI to access the scintillation kinetics of the prompt component resulting from the radiative recombination of DPA singlet states S_1^* (Figure S8). In all samples, the scintillation intensity decays as a single exponential function with a lifetime of <20 ns. In accordance with the results obtained under UV excitation, the addition of porphyrins decreases the DPA fluorescence decay time. The effect is more pronounced as the porphyrin concentration increases. The longer decay lifetime of DPA fluorescence under γ-ray excitation compared to the one under UV excitation is consistent with previous findings and it is ascribed to a local polarization of the solvent around the excited dyes during the scintillation process, and a concomitant change of the oscillator strength of the radiative $S_1^* - S_0$, as recently observed for other blue-emitting scintillating dyes [8, 41].

The waveforms extracted from the neutron ROI instead exhibit a multi-exponential intensity decay (Figure 5a). Notably, all

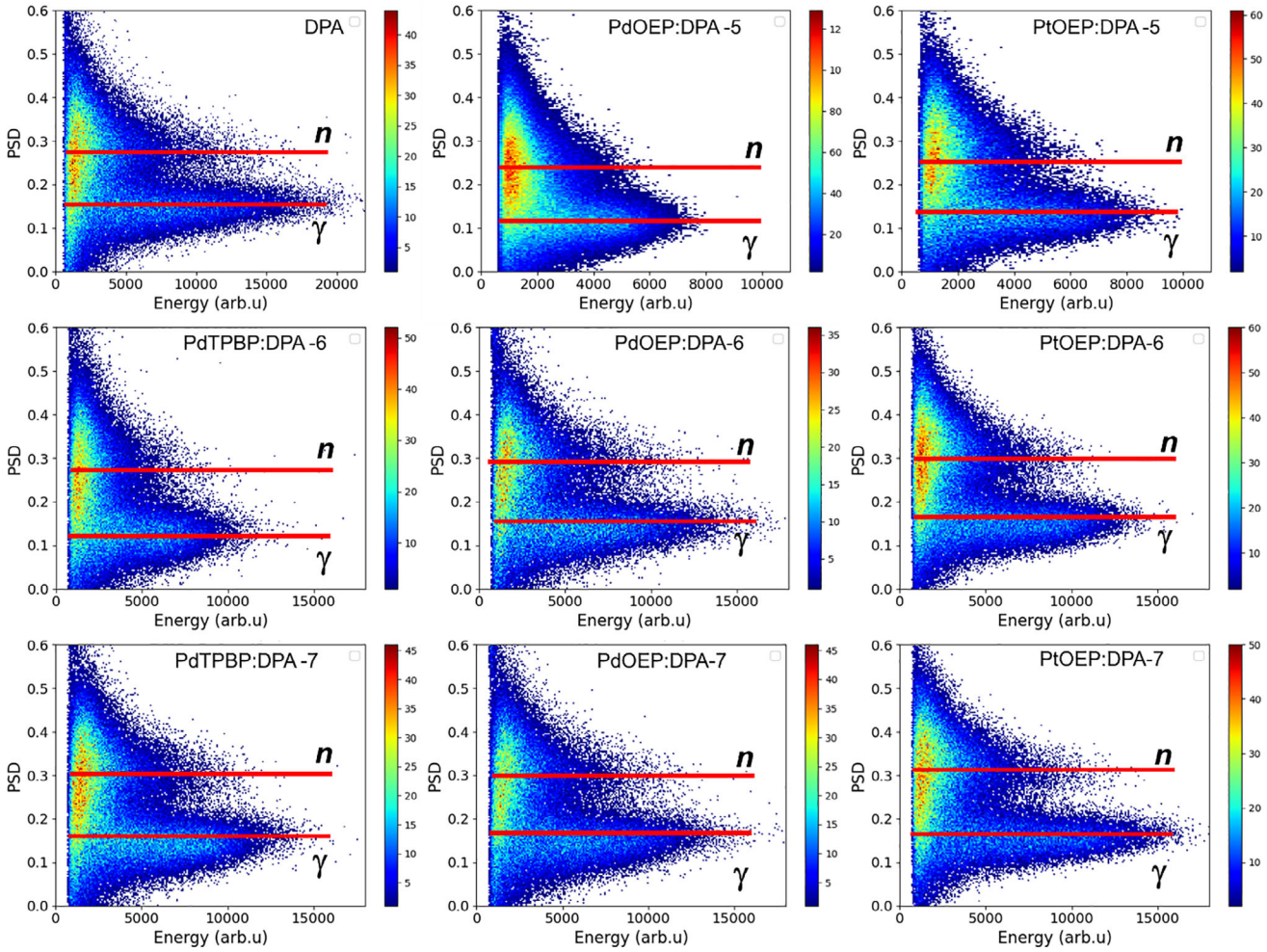

FIGURE 3 | Pulse shape discrimination (PSD) plots of the investigated nanostructured polymer scintillators, recorded under exposure to an AmBe source with an activity of 2 MBq. The concentration of DPA is constant at 1.5×10^{-2} M in all samples. The concentration of the porphyrins is 2×10^{-5} M, 2×10^{-6} M, or 2×10^{-7} M; samples are coded *porphyrin*:DPA-5, -6 and -7, respectively. All concentrations are quoted relative to the overall compositions. The x-axis (*Energy*) reports the energy deposited for each event in arbitrary units. Solid horizontal lines mark the PSD signal relative to neutrons (PSD ca. 0.3) and γ-rays (PSD ca. 0.18).

scintillation signals are exhausted within a time of < 300 ns. The scintillation kinetics were thus analyzed considering two temporal regions. A prompt decay component at short times <20 ns is observed, which corresponds to the radiative recombination of DPA singlet states S_1^*. Additionally, a delayed fluorescence component in the hundreds of nanoseconds time scale, resulting from the TTA occurring in the nanodroplets, can be discerned. The waveform data can be fitted with a multi-exponential decay function, with a fixed fast component extrapolated from the γ-ray scintillation data (Figure S8) to quantify the relative contribution of delayed fluorescence to the total emission. This analysis directly reveals the higher intensity of the delayed fluorescence at time-zero (Δ_{DF}) in the presence of the metalated porphyrins, shown in the insets of Figure 5a and Table S6, which mirrors an increased initial population of annihilating triplets ΔT_1^* (Section S2).

At a sensitizer concentration of 2×10^{-5} M, no data can be reported for the PdTPBP-based material due to its weak light output. A Δ_{DF} of +100% is achieved using PtOEP, corresponding to a $\Delta T_1^* = +43\%$. Conversely, the more efficient triplet BET toward PdOEPs, amplified in the confined droplet, reduces the DPA triplet population, hindering any sensitization [30].

At a sensitizer concentration of 2×10^{-6} M, scintillation light is observed for all compositions. The materials comprising PtOEP and PdOEP show the same sensitization ability with a $\Delta_{DF} \sim +50\%$, which corresponds to an increment $\Delta T_1^* \sim +22\%$ in the number of annihilating triplets. Notably, a large increase in $\Delta_{DF} = +230\%$ is observed for PdTPBP, in accordance with the material's excellent Δ_{PSD} value discussed above. This increment mirrors a significant excellent triplet sensitization effect with a ΔT_1^* as high as +80%. We ascribe this result to the different electronic structures of the employed porphyrins. Both PtOEP and PdOEP are excellent triplet sensitizers for DPA by TTET, but their effective triplet energy resonances may also cause BET from the DPA triplets to the sensitizer instead of annihilating [30, 42]. This process could create an energy-transfer loop for the triplet exciton, which, over long times, favors its non-radiative dissipation.

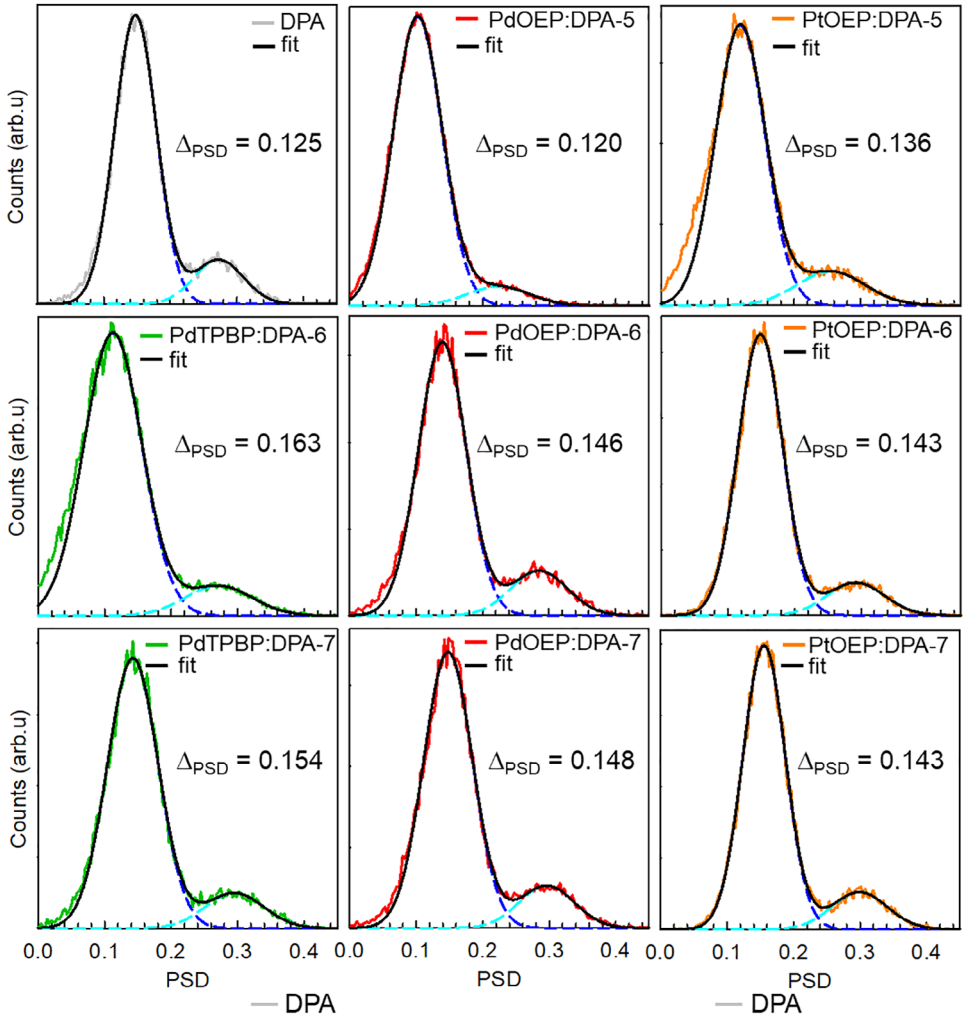

FIGURE 4 | Projection histograms on the *y*-axis of the PSD plots of the nanostructured polymer scintillators reported in Figure 3. The concentration of DPA is constant at 1.5×10^{-2} M in all samples. The concentration of the porphyrins is 2×10^{-5} M, 2×10^{-6} M, or 2×10^{-7} M; samples are coded *porphyrin*: DPA-5, -6 and -7, respectively. All concentrations are quoted relative to the overall compositions. Continuous black lines represent a double Gaussian function fitted to the data. Dashed blue and light blue lines represent the individual Gaussian functions employed for the fit of γ-rays and neutrons peaks, respectively. The parameter Δ_{PSD} is calculated as the difference of the PSD values corresponding to the two maxima of the Gaussian functions. The associated uncertainty is ± 0.001.

We note that for the employed porphyrin concentrations, the triplet BET is negligible in conventional solutions, where an infinite space is available for diffusing triplets. However, the nanoconfinement in the present materials favors this energetic pathway, because of the forced proximity of excited DPA and sensitizer molecules, which makes triplet BET and TTA rates competitive. Indeed, in the case of the PdTPBP sensitizer, the triplet BET is energetically forbidden; thus, any additional DPA triplet generated by the presence of heavy metal atoms can be exploited for TTA to generate a more intense delayed emission and therefore achieve a better PSD. These experimental results show that a too large resonance between the triplet of sensitizers and annihilators is, in contrast to our original expectations, detrimental to the global PSD performance.

In the samples with the lowest sensitizer concentration of 2×10^{-7} M, the Δ_{DF} upon adding the sensitizers is more moderate, with values of 46%, 55%, and 76% for PtOEP, PdOEP, and PdTPBP, respectively. The trend follows again the triplet BET probability, supporting our picture. The observed Δ_{DF} values correspond to a ΔT_1^* of +21%, +24% and +33%, respectively.

The TTA kinetics in the nanostructured scintillators were further investigated by decoupling the delayed emission component. Figure 5b shows the delayed fluorescence signal originating from TTA, decoupled from the prompt component ascribed to the direct excited singlets recombination (Table S6, Section S1). Due to the confinement of excited molecules in a structure much smaller than the triplet diffusion length in organic solvents [29], we can assume to be in rapid diffusion limit, thus the TTA kinetics can be expressed by: [18]

$$k_{TTA} = 8\pi D R_{TT} \left[T_1^*\right] \quad (1)$$

where D is the diffusion coefficient of the solvent, $R_{TT} \sim 1$ nm is the distance at which TTA can occur, and $[T_1^*]$ is the density of available triplets [43, 44]. Notably, the minimum k_{TTA} rate of 0.25 MHz in the nanodroplets (Section S2) is an order of

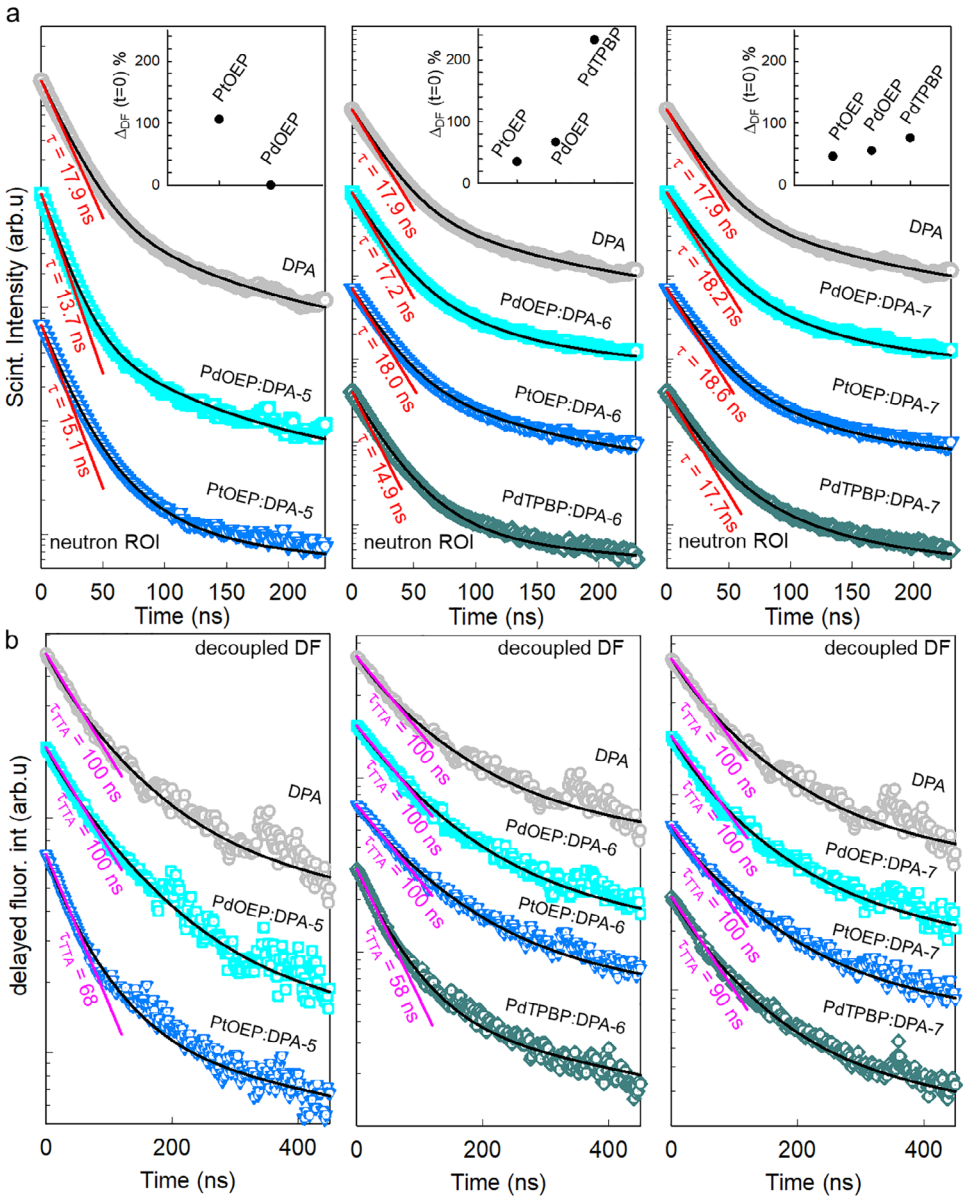

FIGURE 5 | a) Averaged normalized scintillation waveforms of the nanostructured polymer scintillators taken from the neutron ROI (region of interest) in the PSD plots reported in Figure 3. The concentration of DPA is constant as high as 1.5×10^{-2} M in all samples. The concentration of the porphyrins is 2×10^{-5} M, 2×10^{-6} M, or 2×10^{-7} M; samples are coded *porphyrin*:DPA-5, -6 and -7, respectively. All concentrations are quoted relative to the overall compositions. The insets in panel (a) show the relative increase of the delayed fluorescence intensity at time-zero (Δ_{DF}) in the presence of metalated porphyrins, calculated from the fit of the waveforms with a multi-exponential decay function (solid black lines, Table S6). Solid red lines are the fast single exponential decay function used in the fits to account for the prompt emission contribution taken from the fit of the waveforms extracted from the γ-rays ROI (Supporting information Figure S8, Table S6). b) Delayed fluorescence pulses decoupled from the prompt emission. Solid black lines are the fit of data with a multi-exponential decay function. Pink lines are the first single exponential decay component derived from the fit that mirrors the fast TTA in the nanodroplets.

magnitude larger than the spontaneous decay rate of the DPA triplets in the kHz range, thus all the confined triplets decay through TTA when at least two are simultaneously present in the same droplet. In this regime, the first mono-exponential component of the decoupled delayed fluorescence decay, mirrors the initial fast TTA kinetic with a characteristic lifetime $\tau_{DF} = \tau_{TTA} = (k_{TTA})^{-1}$. The DPA-only reference sample shows a k_{TTA} of ~10 MHz, consistent with the confined-TTA model used here to describe the kinetic of the investigated nanostructured polymers. In agreement with the results discussed above, at a PtOEP concentration of 2×10^{-5} M a faster TTA kinetic is observed, with k_{TTA} ~15 MHz ($\tau_{TTA} = 68$ ns). From Equation (1), this corresponds to a $\Delta T_1^* = 47\%$ in the triplet density, in perfect agreement with the previous result. Conversely, no significant change can be observed for PdOEP as no effective sensitization occurs. At a sensitizer concentration of 2×10^{-6} M, only the PdTPBP-containing sample shows an evident increase of the k_{TTA} rate up to ~17 MHz ($\tau_{TTA} =$ 58 ns), a value that is almost doubled with respect to the un-sensitized scintillator and in agreement with the significant sensitization of the initial number of annihilating triplets

$\Delta T_1^* = 73\%$, again in agreement with the value discussed above. This means that the scintillation signal is effectively exhausted within a time window of 200 ns, thus allowing the PSD analysis for counting rates larger than 1 MHz. Conversely, no evident effect on TTA kinetics can be observed with PdOEP and PtOEP following their limited sensitization ability of the DPA triplet population that does not affect the TTA kinetics dramatically (Figure S10). At a concentration of 2×10^{-7} M, as expected, only the PdTPBP still induces a slight but detectable increase of k_{TTA} up to 11 MHz ($\tau_{TTA} = 90$ ns) because only the $\Delta T_1^* = +33\%$ leads to a small but still detectable variation of the TTA kinetic.

3 | Conclusion

To summarize, we investigated a series of nanostructured scintillators for γ/neutron PSD which exploit the sensitized TTA-based delayed fluorescence univocally generated upon neutron interaction to discriminate them from the prompt scintillation generated by γ-rays. The scintillators contain nanoscale liquid droplets homogenously distributed in a polymeric matrix. These droplets only contain DPA as a TTA-active emitter and one of three phosphorescent metalated porphyrins as triplet sensitizers, which are present at different concentrations. The spectroscopic and scintillation experiments highlighted multiple effects due to the presence of the metalated porphyrins packed in close proximity to the annihilators/emitter dyes while encapsulated in the liquid nanodomains. Surprisingly, the best γ/neutron discriminator is the scintillator containing, as sensitizer, the porphyrin whose phosphorescence is completely off resonance with respect to the annihilator/emitter triplet, thus completely hindering the triplet sensitization by non-radiative energy transfer. The highly resonant and thus TTET active metalated porphyrin should generate more annihilator/emitter triplets thanks to the energy transfer. However, due to the strong confinement of dyes, both forward and backward transfer between sensitizers and DPA are possible, thus resulting in a global loss of efficiency and discrimination ability. The observed discrimination improvements, together with the kinetic analysis highlighting the increased formation of annihilator/emitter triplets in the presence of a metalated porphyrin, suggest that the presence of heavy metals in the porphyrin promotes singlet-to-triplet intersystem crossing on DPA during the scintillation mechanism by an intermolecular heavy-atom effect, while TTET plays a negligible role.

In the best composition, which limits trivial self-absorption and luminescence quenching, we almost doubled the triplet density created in the nanodroplets, with a corresponding increase of the TTA rate of more than 70% with respect to the reference sample without metalated porphyrin. This enables the system to work in a time window of about 200 ns. The optimized TTA-sensitization improved the system time discrimination by 30% compared to the reference prototype material, surpassing commercially available systems. Moreover, the achieved fast response enables measurements at high counting rates in the MHz range, as demonstrated with high-activity sources (Figure S9, Experimental Section). These results demonstrate that the triplet population of the annihilator dye can be readily increased by incorporating a heavy-metal complex, thereby enhancing the scintillator's time response and discrimination ability. Moreover, the data suggest that a further tailored engineering of these systems, for example by including heavy but optically inert nanoparticles in the droplets, can be a decisive strategy to fully exploit the peculiar photophysics of TTA in confined structures and achieve faster and more sensitive γ/neutron discriminators operating on the ten-nanosecond time scale.

4 | Experimental Section

4.1 | Preparation of the Nanostructured Polymer Scintillators and Reference Material

All chemicals were purchased from Frontier Scientific, Inc., Sigma–Aldrich, ABCR or Tokyo Chemical Industry Co. Ltd. (TCI) and were used as received without further purification. The nanostructured polymer scintillators and the nanostructured reference materials were prepared by adapting previously reported methods [25] under ambient conditions without prior deoxygenation of the single components or their mixtures. The polymer matrix components cetyltrimethylammonium chloride (250 mg), methacrylic acid (665 mg), triethylene glycol (750 mg), triethylene glycol dimethacrylate (175 mg), and 2-hydroxyethyl methacrylate (2.66 g) were mixed in a 20 mL glass vial equipped with a stir bar. To prepare the reference nanostructured scintillator containing only DPA, DPA (25 mg) and butyl benzoate (500 mg) were added. The mixture was heated in an oil bath to 80°C and stirred for 30 min. The vial was then removed from the oil bath and an aqueous hydrogen peroxide solution (30%, 10 mg) and 2- mercaptoethanol (10 mg) were sequentially added. The mixture was briefly shaken and kept for 2 min before dimethylthiomethane (27 mg) was added and the vial was briefly shaken again. The mixture was filtered through a 0.2 µm PTFE filter and filled into a glass cuvette (external dimensions = 12.5 × 12.5 × 45 mm, optical path length and internal width = 10 mm) that was closed with a stopper. The clear mixture was left to react at room temperature overnight and a hard and transparent glassy material was obtained, which was then released from the glass cuvette for further use. To prepare the nanostructured scintillator containing DPA and the metalated porphyrins, the same process was applied, but instead of only DPA (25 mg) and butyl benzoate, for the metalated porphyrins concentration $c = 2 \times 10^{-5}$ M in final samples, a solution of DPA (25 mg) and PdOEP (85%, 0.075 mg), or PtOEP (95%, 0.073 mg) or PdTPBP (95%, 0.092 mg) in butyl benzoate (500 mg) was added. Lower concentration samples ($c = 2 \times 10^{-6}$ M and 2×10^{-7} M) were prepared using the same method by adjusting the porphyrin mass. To prepare the reference samples with only the metalated porphyrins concentration at $c = 2 \times 10^{-5}$ M a solution of PdOEP (85%, 0.075 mg), or PtOEP (95%, 0.073 mg) or PdTPBP (95%, 0.092 mg) in butyl benzoate (500 mg) was added. Given that the liquid phase occupies 10% of the total volume, the effective concentration inside the droplet is ten times the nominal one employed for the synthesis.

4.2 | Photoluminescence Studies

Time-resolved photoluminescence experiments in the nanosecond time scale were performed by using a pulsed laser LED at 340 nm (3.65 eV, EP-LED 340 Edinburgh Instruments, pulse width 120 ps) as excitation source and an FLS1000 Edinburgh

setup in time-correlated single photon counting (TCSPC) for acquisition.

4.3 | Radioluminescence Studies

Steady-state RL measurements were carried out at room temperature using a homemade apparatus featuring, as a detection system, a liquid nitrogen-cooled, back-illuminated, and UV enhanced charge coupled device (Jobin-Yvon Symphony II) combined with a monochromator (Jobin-Yvon Triax 180) equipped with a 100 lines mm^{-1} grating. All spectra were corrected for the spectral response of the detection system. RL excitation was obtained by unfiltered X-ray irradiation through a Be window, using a Philips 2274 X-ray tube with tungsten target operated at 20 kV. At this operating voltage, a continuous X-ray spectrum was produced by a Bremsstrahlung mechanism superimposed to the L and M transition lines of tungsten, due to the impact of electrons generated through thermionic effect and accelerated onto a tungsten target. The dose rate was 0.2 Gy s^{-1}, evaluated by comparison with a calibrated $^{90}Sr^{90}Y$ beta radioactive source and using optically stimulated luminescence emission from quartz crystalline powder (100–200 μm grains).

4.4 | ^{60}Co Scintillation Measurements

The measurements were performed at the Nuclear Measurement Laboratory at the Institute for Plasma Science and Technology (CNR-ISTP) in Milano. The detectors, made by the scintillation material coupled to the PhotoMultiplier Tube (PMT), were exposed to a ^{60}Co γ-ray source (E = 1.17 MeV and 1.33 MeV). The γ-source was placed in front of the detectors, emitting γ-rays isotropically. The scintillation light was converted into an electrical signal by using a Hamamatsu model R9420-100-10 PMT. The scintillator materials were wrapped with Teflon tape in order to decrease the light loss and to direct the light toward the PMT surface through multiple reflections. The electric signal was then fed into a CAEN DT5730 digitizer, sampling every 2 ns with a 14-bit resolution, recording all waveforms higher than a selectable threshold. Each event was analyzed off-line by calculating the area (Qlong) under a gate as long as the waveform, which is proportional to the total scintillation light produced. The area of each waveform was then used to populate the histogram representing the recorded energy spectrum.

4.5 | Neutron and γ-Ray Detection

Neutron detection experiments were performed at the Nuclear Engineering Division Laboratory at the Department of Energy at Polytechnic of Milan. Here, neutrons were emitted by a source of AmBe. The energy of the emitted neutrons is a broad spectrum distributed between 1 and 8 MeV, peaked at 4 MeV. For this experiment, the detectors were placed in front of the AmBe source at a distance of 15 cm. For the high-rate experiment (Figure S9), the detector was placed in front of a ^{137}Cs γ-rays source at a distance of 140 cm, thus receiving a dose rate of 9.4 mS/h. The neutron contribution was given by a source of AmBe of 2MBq put in contact with the scintillators. This resulted in a counting rate of 1 MHz. The electronic acquisition chain and the analysis tools used for these measurements are identical to the ones used in the previous section (^{60}Co scintillation measurements).

4.6 | Neutron and γ-Ray PSD Offline Analysis

4.6.1 | PSD Plots

PSD plots were generated by performing the charge integration method for the analysis of the recorded scintillation pulses. Once we found the best gates (Short and Long gate) that gave the maximum separation between the two peaks for the reference scintillator with only DPA, we decided to keep them constant for all the scintillators. In this way, PSD values calculated as $1-Q_{short}/Q_{long}$, where Q_{short} and Q_{long} are the integrated charge at short/long times could be compared among all the scintillators.

4.6.2 | PSD Projections

PSD projections along the *y*-axis have been performed in order to make comparisons of the different scintillator's PSD performances, taking signals from a thoroughly selected threshold on the *x*-axis. Since light yield tends to change for scintillators belonging to the same series and among the different concentrations of metalated porphyrins, we needed to be sure that the projected pulses correspond to the same energy spectra of neutrons. To do so, we selected the threshold values so that we considered the same number of neutrons for each scintillator. Effectively, this is equivalent to setting a threshold so that the area under the fitted curve of the neutron peak is the same for all the samples. In this way, PSD capabilities can be safely compared.

4.6.3 | Waveforms Extraction

The reported waveforms for each scintillator have been obtained selecting a given number of signals from the two ROI on the PSD plots associated to the γ-rays and neutrons, normalizing them and then making a single average waveform. The two ROI have been selected at the highest possible values on the x-axes and the selected interval are 5000 values on the *x*-axes and 0.6 on the *y*-axes. In this way we obtained a reasonable number of waveforms to have a good statistic and we are safe from considering confusion regions where it is not possible to state whether the signal comes to the γ-ray or neutron interaction.

Acknowledgements

A.M. and A.E. thank Grant No. H45F2100343000 – MINERVA, LuMIminesceNt scintillating hEterostructures foR advanced medical imaging from the Italian Ministry of University (MUR). C.W. and X.H. acknowledge funding from the Swiss National Science Foundation (Grant No. 200020-197209) and the Adolphe Merkle Foundation.

Open access publishing facilitated by Universita degli Studi di Milano-Bicocca, as part of the Wiley - CRUI-CARE agreement.

Conflicts of Interest

The authors declare no conflicts of interest.

Data Availability Statement

The data that support the findings of this study are available from the corresponding author upon reasonable request.

References

1. R. C. Byrd, J. M. Moss, W. C. Priedhorsky, et al., "Nuclear Detection to Prevent or Defeat Clandestine Nuclear Attack," *IEEE Sensors Journal* 5 (2005): 593–593, https://doi.org/10.1109/jsen.2005.846376.

2. N. Shubayr, "Nuclear Security Measures: A Review of Selected Emerging Technologies and Strategies," *Journal of Radiation Research and Applied Sciences* 17 (2024): 100814, https://doi.org/10.1016/j.jrras.2023.100814.

3. G. Bellini, J. Benziger, D. Bick, et al., "Muon and Cosmogenic Neutron Detection in Borexino," *Journal of Instrumentation* 6 (2011): P05005, https://doi.org/10.1088/1748-0221/6/05/P05005.

4. C. Cazzaniga, P. L. Dapica, K. Ngo, et al., "Characterization Measurements of Compact Neutron Generators of the New NILE Facility," *IEEE Transactions on Nuclear Science* 70 (2023): 1616–1616, https://doi.org/10.1109/tns.2023.3293797.

5. J. B. Birks, *The Theory and Practice of Scintillation Counting* (Pergamon Press, 1964).

6. F. D. Brooks, "Development of Organic Scintillators," *Nuclear Instruments and Methods* 162 (1979): 477–505, https://doi.org/10.1016/0029-554X(79)90729-8.

7. A. Ronchi and A. Monguzzi, "Sensitized triplet–triplet annihilation based photon upconversion in full organic and hybrid multicomponent systems," *Chemical Physics Reviews* 3 (2022): 41301, https://doi.org/10.1063/5.0112032.

8. J. B. Birks, *Photophysics of Aromatic Molecules* (Wiley-Interscience, 1970).

9. T. N. Singh-Rachford and F. N. Castellano, "Photon upconversion based on sensitized triplet–triplet annihilation," *Coordination Chemistry Reviews* 254 (2010): 2560–2573, https://doi.org/10.1016/j.ccr.2010.01.003.

10. A. Monguzzi, J. Mezyk, F. Scotognella, R. Tubino, and F. Meinardi, "Upconversion-induced Fluorescence in Multicomponent Systems: Steady-state Excitation Power Threshold," *Physical Review B* 78 (2008): 195112, https://doi.org/10.1103/PhysRevB.78.195112.

11. S. Mattiello, S. Mecca, A. Ronchi, et al., "Diffusion-Free Intramolecular Triplet–Triplet Annihilation in Engineered Conjugated Chromophores for Sensitized Photon Upconversion," *ACS Energy Letter* 7 (2022): 2435–2442, https://doi.org/10.1021/acsenergylett.2c01224.

12. G. Laustriat, "The Luminescence Decay of Organic Scintillators," *Molecular Crystals* 4 (1968): 127–145, https://doi.org/10.1080/15421406808082905.

13. M. Hamel, *Plastic Scintillators : Chemistry and Applications* (Springer, 2021).

14. N. Zaitseva, A. Glenn, L. Carman, et al., "Pulse Shape Discrimination in Impure and Mixed Single-crystal Organic Scintillators," *IEEE Transactions on Nuclear Science* 58 (2011): 3411–3420, https://doi.org/10.1109/tns.2011.2171363.

15. E. Montbarbon, Z. Zhang, A. Grabowski, et al., "The Role of the Secondary Fluorophore in Ternary Plastic Scintillators Aiming at Discriminating Fast Neutrons From Gamma-rays," *Journal of Luminescence* 213 (2019): 67–74, https://doi.org/10.1016/j.jlumin.2019.04.059.

16. M. Flaska and S. A. Pozzi, "Identification of Shielded Neutron Sources With the Liquid Scintillator BC-501A Using a Digital Pulse Shape Discrimination Method," *Nuclear Instruments and Methods in Physics Research A* 577 (2007): 654–663, https://doi.org/10.1016/j.nima.2007.04.141.

17. M. Hamel, B. Sabot, C. Dutsov, G. H. V. Bertrand, and K. Mitev, "Tuning the Decay Time of Liquid Scintillators," *Journal of Luminescence* 235 (2021): 118021, https://doi.org/10.1016/j.jlumin.2021.118021.

18. A. Ronchi and A. Monguzzi, "Developing Solid-State Photon Upconverters based on Sensitized Triplet–Triplet Annihilation," *Journal of Applied Physics* 129 (2021): 50901, https://doi.org/10.1063/5.0034943/158104.

19. N. Zaitseva, B. L. Rupert, and I. PaweŁczak, "Plastic Scintillators With Efficient Neutron/Gamma Pulse Shape Discrimination," *Nuclear Instruments and Methods in Physics Research A* 668 (2012): 88–93, https://doi.org/10.1016/j.nima.2011.11.071.

20. N. P. Zaitseva, A. M. Glenn, M. L. Carman, et al., "Multiple Dye Interactions in Plastic Scintillators: Effects on Pulse Shape Discrimination," *Nuclear Instruments and Methods in Physics Research A* 978 (2020): 164455, https://doi.org/10.1016/j.nima.2020.164455.

21. T. G. Fox and P. J. Flory, "Viscosity—Molecular Weight and Viscosity—Temperature Relationships for Polystyrene and Polyisobutylene 1,2," *Journal of the American Chemical Society* 70 (2002): 2384–2395, https://doi.org/10.1021/JA01187A021.

22. E. V. Van Loef, J. Glodo, U. Shirwadkar, et al., "Solution Growth and Scintillation Properties of Novel Organic Neutron Detectors," *Nuclear Instruments and Methods in Physics Research A* 652 (2011): 424–426, https://doi.org/10.1016/j.nima.2010.07.072.

23. X. Hu, D. Rigamonti, I. Villa, et al., "Sensitized Triplet–Triplet Annihilation in Nanostructured Polymeric Scintillators Allows for Pulse Shape Discrimination," *Advanced Materials* 36 (2024): 2400443, https://doi.org/10.1002/adma.202400443.

24. R. Vadrucci, A. Monguzzi, F. Saenz, et al., "Nanodroplet-Containing Polymers for Efficient Low-Power Light Upconversion," *Advanced Materials* 29 (2017): 1702992, https://doi.org/10.1002/adma.201702992.

25. F. Saenz, A. Ronchi, M. Mauri, et al., "Nanostructured Polymers Enable Stable and Efficient Low-Power Photon Upconversion," *Advanced Functional Materials* 31 (2021): 2004495, https://doi.org/10.1002/adfm.202004495.

26. F. Meinardi, M. Ballabio, N. Yanai, et al., "Quasi-thresholdless Photon Upconversion in Metal–Organic Framework Nanocrystals," *Nano Letters* 19 (2019): 2169–2177, https://doi.org/10.1021/acs.nanolett.9b00543.

27. T. N. Singh-Rachford and F. N. Castellano, "Pd(II) Phthalocyanine-Sensitized Triplet–Triplet Annihilation From Rubrene," *The Journal of Physical Chemistry A* 112 (2008): 3550–3556, https://doi.org/10.1021/jp7111878.

28. T. Ogawa, N. Yanai, A. Monguzzi, and N. Kimizuka, "Highly Efficient Photon Upconversion in Self-Assembled Light-Harvesting Molecular Systems," *Scientific Reports* 5 (2015): 10882, https://doi.org/10.1038/srep10882.

29. M. Montalti, A. Credi, L. Prodi, and M. T. Gandolfi, *Handbook of Photochemistry* (CRC Press, 2006).

30. D. Meroni, A. Monguzzi, and F. Meinardi, "Photon Upconversion in Multicomponent Systems: Role of Back Energy Transfer," *The Journal of Chemical Physics* 153 (2020): 114302, https://doi.org/10.1063/5.0021253/199615.

31. A. Monguzzi, R. Tubino, and F. Meinardi, "Upconversion-induced Delayed Fluorescence in Multicomponent Organic Systems: Role of Dexter Energy Transfer," *Physical Review B* 77 (2008): 155122, https://doi.org/10.1103/PhysRevB.77.155122.

32. D. R. White, "An Analysis of the Z-dependence of Photon and Electron Interactions," *Physics in Medicine & Biology* 22 (1977): 219–228, https://doi.org/10.1088/0031-9155/22/2/003.

33. I. Villa, B. Santiago Gonzalez, M. Orfano, et al., "The Sensitization of Scintillation in Polymeric Composites Based on Fluorescent Nanocomplexes," *Nanomaterials* 11 (2021): 3387, https://doi.org/10.3390/nano11123387.

34. I. Villa, A. Monguzzi, R. Lorenzi, et al., "On the Origin of the Light Yield Enhancement in Polymeric Composite Scintillators Loaded With Dense Nanoparticles," *Nano Letters* 24 (2024): 8248–8256, https://doi.org/10.1021/acs.nanolett.4c00681.

35. J. R. Lakowicz, *Instrumentation for Fluorescence Spectroscopy* (Springer, 2006), https://doi.org/10.1007/978-0-387-46312-4.

36. M. Inokuti and F. Hirayama, "Influence of Energy Transfer by the Exchange Mechanism on Donor Luminescence," *The Journal of Chemical Physics* 43 (1965): 1978–1989, https://doi.org/10.1063/1.1697063.

37. W. Mengesha, P. L. Feng, J. G. Cordaro, M. R. Anstey, N. R. Myllenbeck, and D. J. Throckmorton, "A Method for Calibrating the Relative Gamma-ray Light Yield of Plastic Scintillators," *Review of Scientific Instruments* 88 (2017): 035108, https://doi.org/10.1063/1.4978288.

38. H. Ito, K. Wada, T. Yano, et al., "Analyzing the Neutron and γ-ray Emission Properties of an Americium–beryllium Tagged Neutron Source," *Nuclear Instruments and Methods in Physics Research A* 1057 (2023): 168701, https://doi.org/10.1016/j.nima.2023.168701.

39. G. Basu, M. Kubasik, D. Anglos, and A. Kuki, "Spin-forbidden Excitation Transfer and Heavy-atom Induced Intersystem Crossing in Linear and Cyclic Peptides," *The Journal of Physical Chemistry* 97 (2002): 3956–3967, https://doi.org/10.1021/J100118A006.

40. Z. S. Romanova, K. Deshayes, and P. Piotrowiak, "Remote Intermolecular "Heavy-Atom Effect": Spin−Orbit Coupling Across the Wall of a Hemicarcerand," *Journal of the American Chemical Society* 123 (2001): 2444–2445, https://doi.org/10.1021/JA002612P.

41. M. Baruah, W. Qin, C. Flors, et al., "Solvent and pH Dependent Fluorescent Properties of a Dimethylaminostyryl Borondipyrromethene Dye in Solution," *The Journal of Physical Chemistry A* 110 (2006): 5998–6009, https://doi.org/10.1021/JP054878U.

42. V. Gray, B. Küçüköz, F. Edhborg, M. Abrahamsson, K. Moth-Poulsen, and B. Albinsson, "Singlet and Triplet Energy Transfer Dynamics In Self-Assembled Axial Porphyrin–Anthracene Complexes: Towards Supra-Molecular Structures For Photon Upconversion," *Physical Chemistry Chemical Physics* 20 (2018): 7549–7558, https://doi.org/10.1039/C8CP00884A.

43. D. D. Thomas, W. F. Carlsen, and L. Stryer, "Fluorescence Energy Transfer in the Rapid-diffusion Limit," *Proceedings of the National Academy of Sciences* 75 (1978): 5746–5750, https://doi.org/10.1073/pnas.75.12.5746.

44. L. Stryer, D. D. Thomas, and C. F. Meares, "Diffusion-enhanced Fluorescence Energy Transfer," *Annual review of biophysics and bioengineering* 11 (1982): 203–222, https://doi.org/10.1146/annurev.bb.11.060182.00122.

Supporting Information

Additional supporting information can be found online in the Supporting Information section.

Supporting File: adfm74937-sup-0001-SuppMat.docx.